Singular continuous spectra in dissipative dynamics

Arkady S. Pikovsky, Michael A. Zaks, Ulrike Feudel, and Jürgen Kurths
Max-Planck-Arbeitsgruppe "Nichtlineare Dynamik," Universität Potsdam, Potsdam, Germany
(Received 28 December 1994)

We demonstrate the occurrence of regimes with singular continuous (fractal) Fourier spectra in autonomous dissipative dynamical systems. The particular example is an ordinary-differential-equation system at the accumulation points of bifurcation sequences associated with the creation of complicated homoclinic orbits. Two different mechanisms responsible for the appearance of such spectra are proposed. In the first case, when the geometry of the attractor is symbolically represented by the Thue-Morse sequence, both the continuous-time process and its discrete Poincaré map have singular power spectra. The other mechanism is due to the logarithmic divergence of the first return times near the saddle point; here the Poincaré map possesses the discrete spectrum, while the continuous-time process displays the singular one. A method is presented for computing the multifractal characteristics of the singular continuous spectra with the help of the usual Fourier analysis technique.

PACS number(s): 05.45.+b

I. INTRODUCTION

The dynamics of nonlinear systems may be described by means of different characteristics. One of the classical (and lately shadowed by more elaborate tools like Lyapunov exponents, dimensions, singularity spectra, etc.) ways to characterize the dynamics of the observable $f(t)$ is to compute its normalized autocorrelation function (autocovariance)

$$C(\tau)=\frac{\langle f(t)f(t+\tau)\rangle}{\langle f^2(t)\rangle} \qquad (1)$$

(the averaging over time and/or the respective set of initial conditions is assumed), which provides the quantitative estimate of the system's ability to return to the same states after regular intervals of time [1–4]. Usually, nonchaotic systems are well correlated: the correlation function of the periodic motion reaches unity at all the integer multiples of the basic period, whereas in the case of the quasiperiodic motion with an irrational ratio of frequencies, the largest peaks correspond to the times proportional to the denominators of successive rational approximations to this ratio, and the amplitudes of these peaks asymptotically approach 1. On the other hand, the eventually (not necessarily monotonously) decaying autocorrelation function of the chaotic motion reflects its property to forget the details of the initial state. As an intermediate stage one may imagine some "not perfectly regular" or "not entirely chaotic" motion for which the correlation function would be everywhere (except for $\tau=0$) separated from 1, but at the same time would not entirely decay, displaying peaks of finite height for arbitrarily large values of τ and thus disclosing the ability of the system to remember "vaguely" its previous history.

Owing to the duality between the autocorrelation function and the Fourier power spectrum, the same statements can be retold in terms of the latter. For both periodic and quasiperiodic processes the Fourier spectrum is obviously composed of discrete delta peaks only; in the former case the peaks are well separated whereas in the latter they are typically dense. The spectrum of the chaotic motion is marked by the presence of a continuous component. In most of the known examples the latter is absolutely continuous with respect to the Lebesgue measure (albeit some local singularities are possible, like in the case of the $1/\omega$ spectrum), but in principle it may also be singular, i.e., be concentrated on a set of Lebesgue measure zero. This singular component might be viewed as some remnant of the discrete ordered-state spectrum in the following way: the response at the frequency corresponding to a singularity (such values must be dense in the spectrum), although not mighty enough to produce a delta peak, is substantially stronger than in the immediate neighborhood. Therefore the singular continuous spectra occupy some intermediate position between the spectra of the well-ordered processes and those of the fully chaotic ones.

Singular continuous spatial spectra have been recently reported for the distributions of particles in systems with incommensurate scales [5–7]. They are also known to appear in quantum systems with quasiperiodic potentials [8] and quasiperiodic external forcing [9,10]. Recently the singular continuous spectra have been observed in dissipative systems with quasiperiodic external forcing, where so-called "strange nonchaotic attractors" (sets which, like chaotic attractors, are not manifolds, but, contrary to them, are characterized by nonpositive Lyapunov exponents) appear [11]. However, to the best of our knowledge no examples of this kind were reported for the conventional autonomous continuous-time dissipative system.

In this paper we show that singular continuous spectra appear in the autonomous system of three ordinary differential equations [12] which resemble very much the Lorenz equations. After reviewing the basic properties of correlations and spectra in Sec. II, we describe the system in Sec. III and present the data which show that singular continuous spectra can be observed at the accumulation

points of the bifurcation scenarios in which the more and more complicated homoclinic orbits of the saddle points are progressively formed and destroyed. Although the scenarios themselves have been studied extensively [12–16], the related unusual correlation properties seem to have been overlooked.

It proves out, that in systems of this kind one encounters at least two different mechanisms, of which each one taken alone already supplies the singular continuous spectrum. One of them is due to the special symmetry (which may either be present or not) of the bifurcation scenario as expressed through the appertaining renormalization rules; as a consequence already the Fourier spectrum produced from the symbolic code of the corresponding orbit displays the required features. The simplest example of such a code is the so-called Thue-Morse [17,18] sequence, for which there exists a rigorous proof of the singularity of the spectral measure. To provide a better understanding of the properties of singular continuous spectra, we will discuss in detail the Thue-Morse sequence as a case study in Appendix A. The other more general mechanism producing a singular continuous spectrum requires no symmetry and is associated with the logarithmic divergence of the return times for the trajectories approaching the homoclinicity. In physical language, variation of return times is tantamount to the phase modulation of the process. The corresponding mathematical model—the so-called special flow—is analyzed in Sec. IV. Finally, the multifractal properties of singular continuous spectra are discussed in Sec. V.

A curious and highly unusual peculiarity of the considered processes is a seeming discrepancy between the continuous flow and its discretization obtained with the help of the Poincaré mapping on a proper surface. As a kind of a counterexample to the conventional belief that the mapping mimics all the dynamical features of the flow, we present and discuss a situation in which the power spectrum of the attractor for the ODE system is singular continuous whereas the Poincaré mapping yields a discrete spectrum. Another example demonstrates different spectral properties of return mappings obtained for two variables in the very same process: the power spectrum is singular continuous for one of them and discrete for the other one.

II. BASIC PROPERTIES OF CORRELATIONS AND SPECTRA

In this section we recall some facts about correlations and spectra (see [19,20]). The autocorrelation function (1) can be represented as a Fourier transform of the spectral measure $\mu(\omega)$:

$$C(t)=\int e^{-i2\pi\omega t}d\mu(\omega) . \tag{2}$$

In general, the spectral measure can be decomposed into the pure point and the continuous component (the possibilities for their simultaneous presence in the spectrum of a continuous-time dynamical system are discussed, e.g., in [21]). In its turn the latter part can be further represented as a sum of the absolutely continuous and the singular continuous components: $\mu=\mu_{\rm PP}+\mu_{\rm AC}+\mu_{\rm SC}$. In the physical language, the pure point component is a set of δ functions (discrete spectrum), while the absolutely continuous component has a spectral density (which is usually called the power spectrum). The singular continuous component unites all what remains after both the pure point and the absolutely continuous components are removed; it sits on a set of zero Lebesgue measure, but is weaker than delta peaks. To evaluate the intensity of the discrete spectrum it proves useful to introduce the averaged squared correlation function as (we assume that the time is discrete, a generalization to the continuous time is straightforward)

$$C_{\rm av}(t)=\frac{1}{t}\sum_{k=0}^{t-1}|C(k)|^2 . \tag{3}$$

According to Wiener's lemma (see [19,20]), the total intensity of the discrete component of the spectrum is $C_{\rm av}(\infty)$. From the other side, a necessary condition for the spectrum to be absolutely continuous is the decay of correlations:

$$\lim_{t\to\infty} C(t)=0 . \tag{4}$$

Hence, calculation of the autocorrelation function allows one (at least in simple cases) to detect singular continuous spectrum. Thus the power spectrum should be singular continuous if $C_{\rm av}(t)$ tends to 0 for large t, while $C(t)$ does not: the former requirement ensures the absence of the discrete component whereas the latter precludes the presence of the absolutely continuous one. We will make use of these criteria in our numerical studies below.

Recently it has been shown that the law of decay of the averaged squared correlation function (3) is related to the correlation dimension D_2 of the spectral measure μ [22–24]:

$$C_{\rm av}(t)\sim t^{-D_2} . \tag{5}$$

Indeed, one can expect that for an absolutely continuous spectral measure having dimension 1 the sum in (3) typically converges, so $C_{\rm av}(t)\sim t^{-1}$ and $D_2=1$, while for a discrete spectrum (zero dimension) $C_{\rm av}$ does not decay and relation (5) gives $D_2=0$.

III. THE ODE SYSTEM, ITS ATTRACTORS, AND THEIR SPECTRA

To demonstrate the action of the mechanisms which produce "intermediate" spectral and correlation properties we use the third order ordinary-differential-equation (ODE) system which is reminiscent of the Lorenz equations:

$$\begin{aligned}\dot{x}&=\sigma(y-x)+\sigma Dy(z-R) ,\\ \dot{y}&=Rx-y-xz ,\\ \dot{z}&=xy-bz+ax ,\end{aligned} \tag{6}$$

but may have different scenarios of transition to chaos. This system (see [12] for the derivation and more detailed description) mimics the averaged thermal convection in the fluid layer subjected to the transversal high-frequency

oscillations of gravity. Vibrations are known to suppress the small-scale fluid motions [25], which makes physically plausible the Lorenz-like truncation to one mode (x) for the velocity field and two modes (y and z) for the temperature distribution. Here σ denotes the Prandtl number of the fluid, R stands for the Rayleigh number (normalized to its critical value in the absence of vibrations), and $b=4\alpha/(1+\alpha^2)$ is the geometrical parameter determined by the wave number α of the convective pattern. The additional (with respect to the Lorenz model) term in the first equation is proportional to the "vibrational parameter" D, given by the squared ratio of the amplitude of the modulation to its frequency; another modification is breaking the symmetry $(x,y)\Longleftrightarrow(-x,-y)$ by means of introduction of the term ax into the third equation.

Similarly to the unperturbed Lorenz equations, the transition to chaos in the equations (6) follows the formation of the homoclinic trajectories to the trivial steady state $x=y=z=0$; in the parameter domain $D<R^{-1}-R^{-2}$ the latter is a saddle point with three real eigenvalues $\lambda_3<\lambda_2<0<\lambda_1$. Whereas in the Lorenz case the positive eigenvalue is larger than the absolute value of the leading (closest to zero) negative one, here the homoclinic bifurcation can be encountered also in the parameter domain

$$\frac{1}{R}-\frac{1}{R^2}-\frac{b(\sigma+1-b)}{\sigma R^2}<D<\frac{1}{R}-\frac{1}{R^2}\,, \tag{7}$$

where $\lambda_2+\lambda_1$ is negative. This means that, as opposed to the Lorenz system, in the vicinity of the saddle point the contraction prevails over the expansion, and the destruction of homoclinic connections should produce not the unstable Ω set [26,27], but stable closed orbits. The further evolution through more and more complicated periodic states eventually leads to the emergence of the chaotic attractor; the structure of the parameter space is enormously rich, with uncountably many different routes to chaos [14–16]. We will focus below on two particular scenarios which seem to be the best suited for the illustration of the unusual spectral and correlation properties. In our computations we will fix the "canonical" Lorenz parameter values $\sigma=10$ and $b=\frac{8}{3}$.

A. Symmetrical case

Let us fix $a=0$, and increase R keeping D in the domain (7). Owing to the symmetry $(x,y)\Longleftrightarrow(-x,-y)$ the homoclinic bifurcation results in the gluing of two mutually symmetrical stable closed orbits into a single one [Figs. 1(a) and 1(b)]. The further sequence consists of the alternating symmetry-breaking bifurcations and subsequent homoclinic gluings of periodic orbits [Figs. 1(c) and 1(d)]. The number of loops of the attracting periodic orbit is doubled at each homoclinic bifurcation (this is not, however, period doubling in the usual sense, since the time period is infinite at the bifurcation point), and the whole bifurcation sequence is converging at the universal geometric rate. The renormalization treatment of the corresponding one-dimensional discontinuous map [13,12] shows that the convergence rate (along with the other scaling characteristics of this hierarchical process)

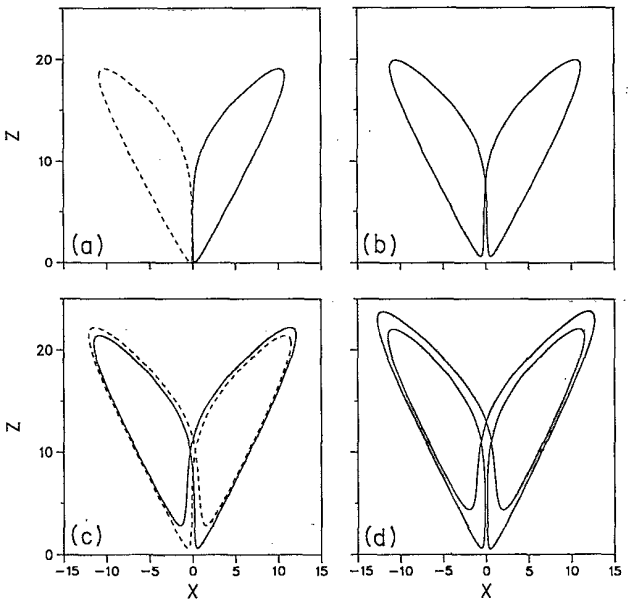

FIG. 1. A sketch of the homoclinic-doubling bifurcation in the system (6): the two symmetrical stable cycles (a) glue into a homoclinic orbit, which produces the stable symmetrical cycle (b); this cycle loses its symmetry with creation of two two-loop stable cycles (c); these cycles glue and produce a "period-4" stable cycle (d).

is entirely determined by the so-called saddle index—the ratio of the eigenvalues $\nu=-\lambda_2/\lambda_1$. The two-dimensional (2D) projection of the resulting symmetric attractor at the accumulation point of homoclinic bifurcations (for $R=15.823\,736\,6\ldots$, $D=0.052\,634\,9\ldots$ which corresponds to $\nu=2.0$) can be seen in Fig. 2. Further increase of R leads to the onset of chaos.

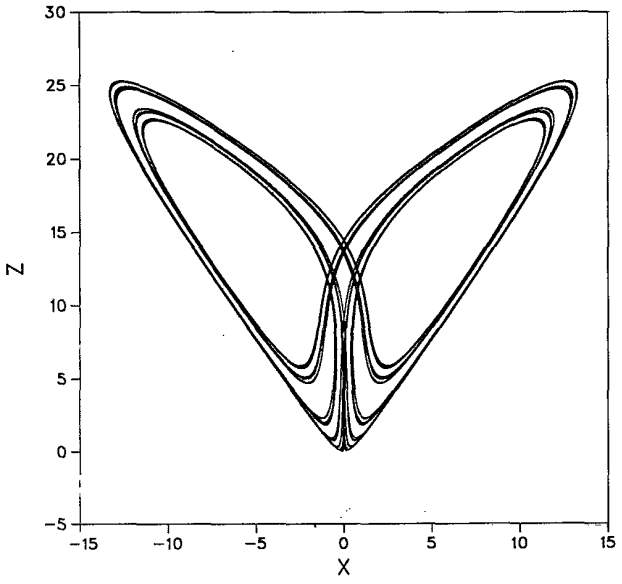

FIG. 2. The view of the attractor of the system (6) at the point of transition to chaos through homoclinic doublings. The Cantor structure of the attractor is clearly seen.

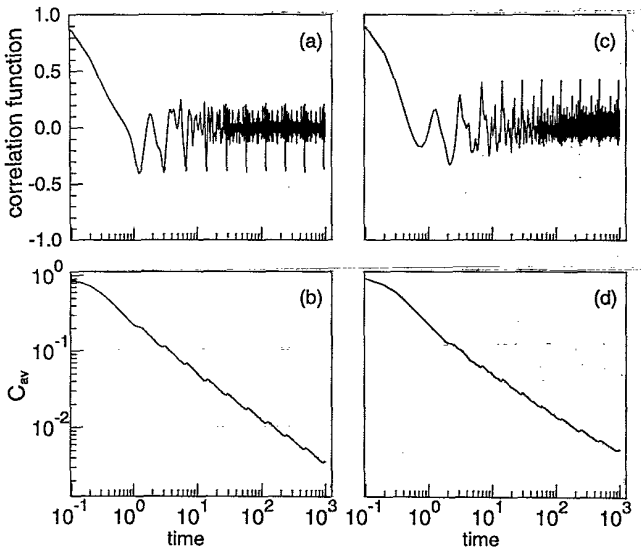

FIG. 3. The autocorrelation functions for the variables x (a) and z (c). Note the logarithmic scale of the time axes. This shape with arguments of the peaks forming a geometrical progression is typical for processes with singular continuous spectra. The averaged squared correlation functions (3) are presented in (b) and (d), respectively.

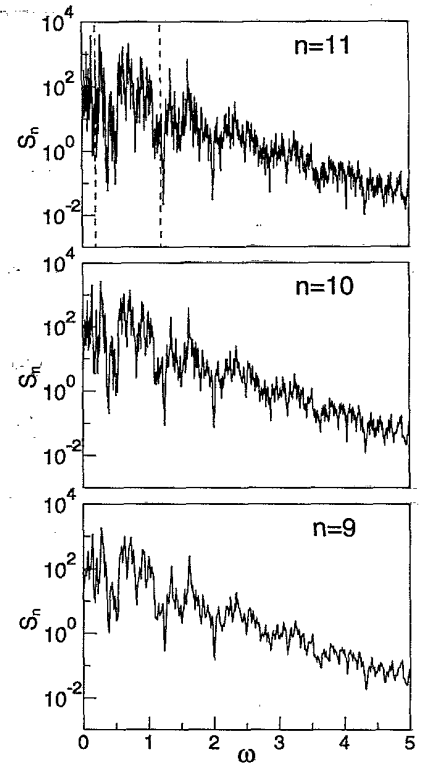

FIG. 4. The power spectrum of the variable x, calculated using the standard method [45] for different numbers of points in the spectrum $N=2^n$. With the increase of N the spectrum becomes more scarred: both the peaks and the depressions grow. The region between the dashed lines is used for determining the multifractal properties of the spectrum in Sec. V.

We now consider the spectral and correlation properties of the system (6) at the transition point. The computed autocorrelation functions for the variables x and z on this attractor are presented in Fig. 3. It can be seen that their shape satisfies the conditions for the spectrum to be singular continuous: the correlations themselves do not decay, so condition (4) is not satisfied; on the other hand, the averaged squared correlation function decays as a power law. The plotted data display a remarkable feature: the values of time corresponding to the largest peaks of $C(t)$ form a geometrical progression; the ratio of the times is approximately 2. This factor corresponds to the fact that the attractor is created through homoclinic doublings. However, unlike in the case of the usual period doublings, the level of correlation remains less than 0.5.

The spectral sums S_n for the same attractor, which were computed with the use of 2^n-point fast Fourier transform (FFT) [at a sampling rate 0.1 in the units of dimensionless time of (6)], and subsequent averaging for many realizations, are presented in Fig. 4. One notices both the "fractalization" of the spectrum with the growth of n and the apparent self-similarity in the low-frequency part of the power spectrum: $S_n(\omega) \propto S_{n+1}(\omega/2)$ (Fig. 5). [The explanation of this self-similarity is given in Appendix A, see Eq. (A3)].

A common way of reduction of a continuous-time dynamical system to a discrete one is to consider the Poincaré map on some surface. For the equations (6) it is convenient to introduce this surface near the saddle as depicted in Fig. 6. Because of the strong volume contraction the resulting Poincaré map can be viewed as quasi-one-dimensional, see Fig. 7. The mapping for the vari-

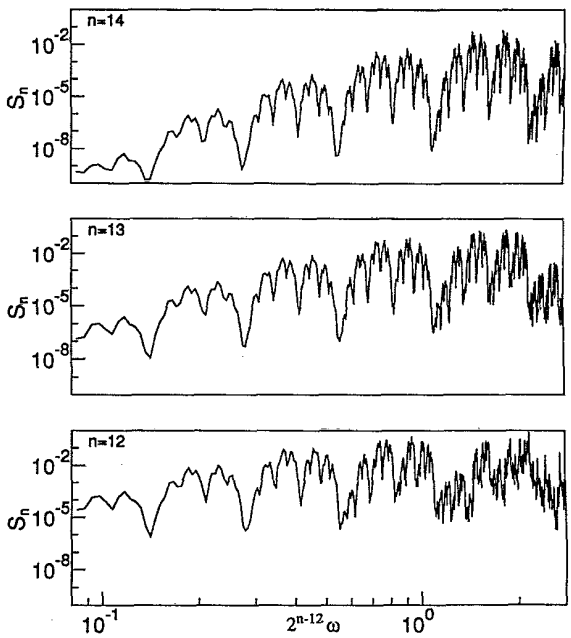

FIG. 5. The low-frequency parts of the spectra of Fig. 4, redrawn in scaled coordinates to show self-similarity.

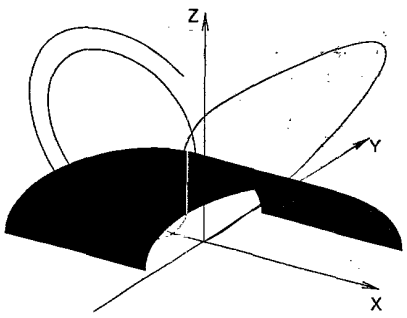

FIG. 6. The sketch of the surface of section (the cylinder $z^2+y^2=81$) used to construct the Poincaré map in the system (6).

able x [Fig. 7(a)] is symmetric and discontinuous due to the symmetry of the underlying ODE system; in the case of the variable z [Fig. 7(b)] which does not participate in the symmetry transformation, the mapping is continuous and has a minimum. Owing to the Cantor-like structure of the attractor, the points do not fill the lines, but these

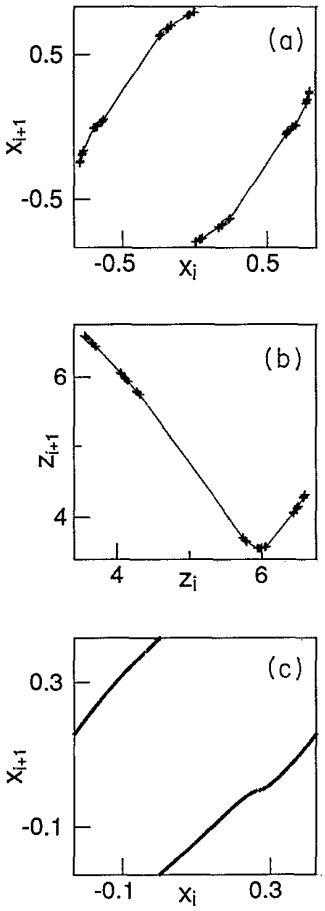

FIG. 7. The Poincaré maps for the variables x (a) and z (b), obtained with the surface of section Fig. 6 for the attractor Fig. 2 (the variable x is additionally projected on a line transversal to the stable manifold of the saddle). The points of the attractor are marked with crosses which are connected by interpolation curves. The mapping (c) corresponds to the attractor Fig. 9; here a quasiperiodic orbit is dense on the interval.

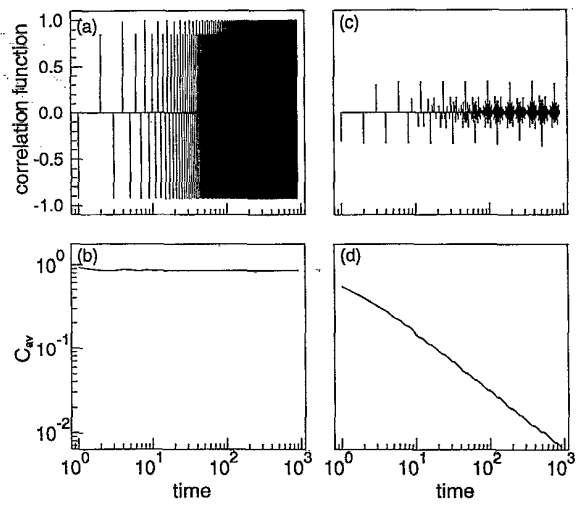

FIG. 8. The correlation function for the discrete sequences x_n (a) and z_n (b). While the power spectrum of x_n remains singular continuous, the power spectrum of z_n is discrete.

can be easily interpolated [13,12]. Calculations of the correlation function $C(n)$ (where the discrete time variable n stands for the number of intersections with the secant) for the corresponding series of the section coordinates, demonstrates that while the spectrum for the values of x remains singular continuous [Fig. 8(a)], the spectrum for z is discrete [Fig. 8(c)] precisely in the same way as it should be for the logistic mapping at the Feigenbaum point [28]. This discrepancy between the properties of two coupled variables stemming from the same dynamical system will be discussed in Sec. III C below.

B. Asymmetrical case

Of many different scenarios which are possible for $a\neq 0$ we take the one which resembles very much the transition to chaos through quasiperiodicity. Without going into details (see [14–16,29]) we should only mention that in the proper parameter domain one can define the "rotation number" ρ, which for the closed periodic orbit is the ratio of the number of loops in the half-space $x>0$ to the entire number of the loops. For the nonclosed orbit ρ is the ultimate "proportion" of these loops, i.e., the limit of the respective ratio for $t\to\infty$. The parameter space can be separated into the "subcritical" domain for which ρ is independent of the initial conditions, and the supercritical domain where orbits with different values of ρ may coexist and one should speak rather about the rotation intervals. These two domains are separated by a "critical" surface. For the parameter plane the latter is just a curve, and the subcritical domain is a union of the countable number of "resonant tongues" inside which ρ is rational and the continuum of curves which correspond to irrational values of ρ. This structure is reminiscent of the Arnold tongues for the circle mappings; however, in our case all the tongues and all the irrational curves emanate from one and the same point; another difference is that at the edges of the tongues the periodic orbits are not necessarily coalescing via the tangent bifurcation, but may also

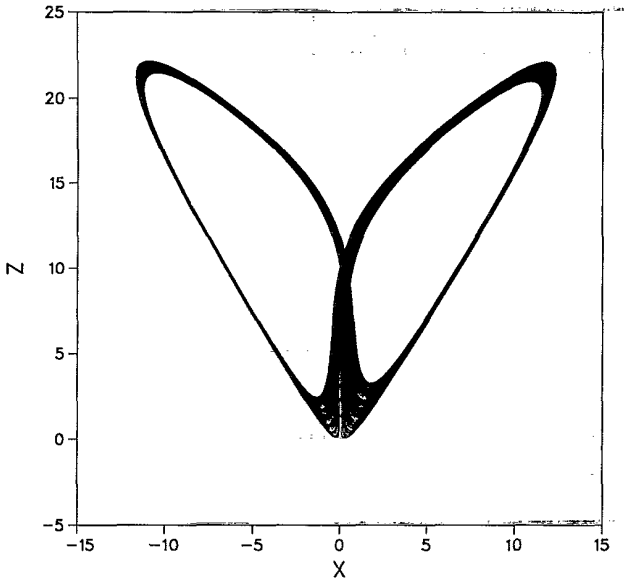

FIG. 9. The view of the attractor of the system (6) at the point of transition to chaos through "quasiperiodicity."

disappear through the formation of the multiturned homoclinic orbit.

Let us fix some irrational value of ρ and move on the parameter plane along the corresponding curve towards the critical line. The respective attracting set at the critical point of transition to chaos for the "reciprocal golden mean" rotation number $\rho=(\sqrt{5}-1)/2$ is presented in Fig. 9; the parameter values $R=14.148\,796\,8\ldots$, $D=0.054\,334\,76\ldots$, $a=-0.561\,127\,33\ldots$ correspond to $\nu=1.5$. One sees that, in contrast to the Cantor-like attractor from Fig. 2, this set looks dense on the transversal section. The Poincaré section resembles very much the critical circle map (with the only difference that the singularity is generally not cubic, but has an order ν) [16,29] insofar as the rotation number is irrational, the attracting orbit is everywhere dense on the interval [Fig. 7(c)]. Correspondingly, the spectrum of the variable x_n discretized in this way contains the pure-point component only. However, the calculation of the autocorrelation function of the underlying continuous-time process $x(t)$ (Fig. 10) demonstrates that its power spectrum is singular continuous.

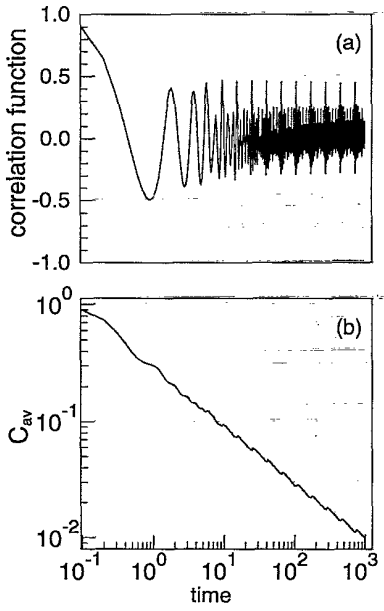

FIG. 10. The autocorrelation functions for the variable x of the attractor Fig. 9. It has typical form for the case of singular continuous spectrum with peaks forming a geometrical progression. The factor of this progression is the golden mean, according to our choice of the rotation number.

C. Two mechanisms for the singular continuous spectrum

The numerical results presented above suggest that at least two distinct mechanisms are responsible for the appearance of singular continuous spectra.

The first mechanism is the one which ensures the singular continuous spectrum for the variable x in the symmetric case. Producing the same results for both the continuous flow and the sequence of the Poincaré sections, it obviously does not depend on the dynamical time properties of the process, and hence may be called the geometric mechanism. Not only the reduction to the mapping, but also the symbolic representation of the orbit of such mapping possesses the same spectral properties. Let us ascribe the symbol L (R) to each loop in the half-space $x<0$ $(x>0)$. On the symbolic language each homoclinic bifurcation is the gluing of some finite symbolic sequence with its mirror counterpart (the same sequence in which all R's are substituted by L's and vice versa). Thereby the scenario of the change of the attractor's code is

$$R \rightarrow RL \rightarrow RLLR \rightarrow RLLRLRRL \rightarrow \cdots .$$

The resulting infinite symbolic code which is obviously invariant under the transformation $R \rightarrow RL$, $L \rightarrow LR$ is known as the Thue-Morse sequence [17,18]. From the mathematical literature it is well known that this sequence has a singular continuous Fourier spectrum [20] (see Appendix A for a detailed discussion). There exists a number of studies on the applications of the Thue-Morse sequence to different physical systems [30–32], however, to our knowledge in all of these examples the sequence was prescribed externally—either as external forcing or as a prepared pattern of the lattice. In our case this sequence appears as a result of the intrinsic dynamics of the system, which owes to the symmetry of the original equations. The correlation and spectral properties of this symbolic code are readily transferred to the values of the Poincaré sections for the variable x and, finally, to the continuous process $x(t)$.

Along with the described scenario which yields the "pure" Thue-Morse sequence, one can follow in the parameter space certain other bifurcational sequences where the geometric mechanism is at work. We will briefly mention just two possibilities. For the general asymmetric case each intersection on the parameter plane of two curves corresponding to the formation of mul-

tilooped homoclinic orbits produces the pencil of lines marking the secondary homoclinic bifurcations [15,16]. Let the symbolic codes of the primary multilooped orbits be two words of some finite (and not necessarily equal) length l_1 and l_2 respectively, the first letter being R in one of them and L in the other. Since the codes of the new homoclinic orbits are obtained by concatenation of these two words, it is straightforward to redefine the coding rules: let us take two given words as the initial blocks and denote them by R and L, respectively. Now one may trace the new sequence of homoclinic doublings [the corresponding orbits have $(l_1+l_2)2^{n-1}$ loops] and locate at some distance its accumulation point, where the symbolic code of the attracting trajectory can be reduced to the conventional Thue-Morse form by the single symbolic renormalization.

The other example is provided in the symmetric case $a=0$ by the sequences of "homoclinic m-tuplings," which converge to the parameter values where the symbolic code is invariant with respect to the substitution $R\to RL^{m-1}$, $L\to LR^{m-1}$. For $m=2$ one gets the scenario of homoclinic doublings described above, which provides the Thue-Morse code; symbolic sequences for the higher values of m also demonstrate singular continuous spectral properties, and this is immediately mirrored by the corresponding characteristics of the trajectories for the continuous flow (6).

It is noteworthy that one can find the Thue-Morse sequence even in a much simpler dynamical system: consider the symmetrical cubic mapping $x\to ax(x^2-3)$. This mapping has three intervals of monotonicity: $x<-1$, $-1<x<1$, and $x>1$, which provides the natural coding by the symbols L, C, and R, respectively. For the particular choice of the parameter $a=0.965\,941\,391\ldots$ the stable orbit starting at the point $x=1$ does not visit the central segment, and its symbolic coding which is composed of R's and L's only is organized into the Thue-Morse sequence. No wonder that at this parameter value the Fourier spectrum of the attracting trajectory for the continuous cubic mapping is singular continuous.

The second mechanism which ensures the onset of singular continuous spectra is at work for the variable z in the symmetric case and for all the variables in the absence of symmetry. Here the discretized and the continuous-time processes have qualitatively different spectra. The reason for the difference must lie in the properties of the return times between the consecutive Poincaré sections; therefore it is natural to call this mechanism the dynamical one. Indeed, the Poincaré map for the considered ODE system, as well as for the Lorenz equations, is singular: it is not defined at the intersection of the secant surface with the stable manifold of the saddle point. The behavior of return times is also singular: as the point of section approaches the stable manifold, the return time diverges logarithmically. As a result one cannot speak about the characteristic return time (as it would be the case for period doublings); insofar as the orbit should pass arbitrarily close to the saddle point, the return time may be arbitrary large. We conjecture that this singularity is responsible for the singular continuous nature of the spectrum. To support this conjecture we perform in the following section the analysis of the idealized dynamical system—the so-called special flow.

IV. THE SPECIAL FLOW

In this section we intend to demonstrate that the logarithmic singularity of the return times alone provides the singular continuous spectrum. For this purpose we consider an idealized process, for which it is possible to separate properties of the Poincaré map and of the return times. The construction we use is a variant of the so-called special flow, typically used in studies of ergodic properties of continuous-time dynamical systems [19]. The special flow over the map $x\to f(x)$ of the interval $0\le x<1$ is defined as follows. Consider the piece of the plane $0\le x<1$, $0\le y<F(x)$. The trajectory starting from the initial point $x(0),y(0)$ is defined as

$$\begin{aligned} x(t)&=f^n(x(0))\,,\\ y(t)&=y(0)+t-\sum_{k=0}^{n-1}F(f^k(x(0)))\,, \end{aligned} \tag{8}$$

where integer n as a function of continuous time t is uniquely defined from the inequalities

$$\sum_{k=0}^{n-1}F(f^k(x(0)))\le y(0)+t<\sum_{k=0}^{n}F(f^k(x(0)))\,.$$

The geometrical representation of the special flow is the following (see Fig. 11): a trajectory moves on the plane x, y upwards with unit velocity, until the value of y reaches the border $y=F(x)$, then the trajectory jumps to the point $(f(x),0)$ and begins to move upwards again. One can see that the special flow has the map $x\to f(x)$ as the Poincaré map, and the return times are given by the function $F(x)$.

The variable x can be considered as the amplitude and the ratio $y/F(x)$ as the phase of the continuous-time dynamical process. The amplitude modulation is determined by the Poincaré map, while the phase modulation depends also on the properties of the return times $F(x)$. By choosing an observable which depends only on the phase, e.g., $w=\cos[2\pi y/F(x)]$, we can select properties of the continuous dynamics that are connected with the

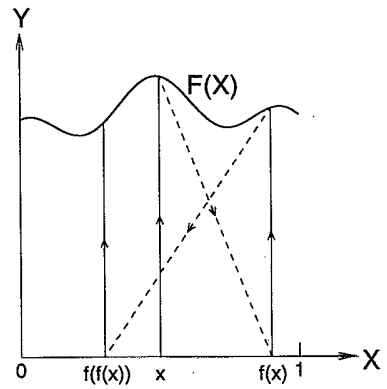

FIG. 11. The geometrical representation of the special flow construction.

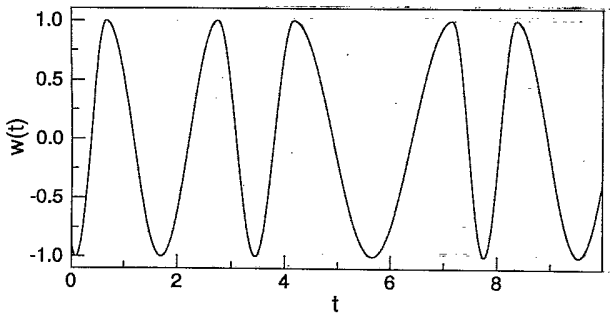

FIG. 12. The process with pure phase modulation, generated with the special flow.

distribution of the return times: for this observable the amplitude modulation vanishes (see Fig. 12). These properties are completely defined by the Poincaré map $x \to f(x)$ and by the function $F(x)$. We consider the following two cases:

(1) $f(x)$ is the Feigenbaum map at the point of transition to chaos [33].

(2) $f(x)$ is a circle map with irrational rotation number.

In both cases the spectrum of the Poincaré map of the variable x is discrete. While with a smooth function $F(x)$ the spectrum of the variable w remains discrete [34,35], it can become continuous if F is singular. Von Neumann proved in [36] that in the second case a discontinuous $F(x)$ can generate a process with continuous spectrum. The mixing properties of the special flow when the function F has a logarithmic singularity $F(x) \sim -\log|x-x_0|$ were studied in Refs. [37,38]. However, to the best of our knowledge, the characteristics of the Fourier spectrum have not been considered.

We have investigated numerically the correlation properties of the process $w(t)$ in the presence of a logarithmic singularity for cases (1) and (2) described above (a renormalization group analysis of this problem is now in progress). The results are presented in Fig. 13. They clearly demonstrate, according to the criteria discussed in Sec. II, that special flows with a logarithmic singularity have singular continuous spectra. It seems that for the circle map, where trajectories are dense on the interval, the location of the logarithmic singularity is irrelevant. For the Feigenbaum map the attractor is a Cantor set, so the singularity should not fall in a gap. In order to model the ODE system close to the homoclinicity, the singularity must be placed at the extremum of the map, and this point belongs to the Feigenbaum attractor.

Thus, consideration of special flows allows us to conclude that a logarithmic singularity in return times can provide a singular continuous spectrum, even if the spectrum of the Poincaré map itself is discrete. For the system of ODEs considered above, this mechanism works for the variable z in the symmetrical case, and in general in the asymmetrical case.

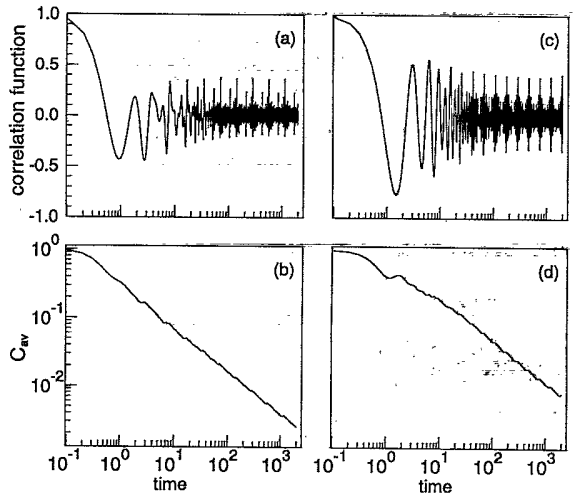

FIG. 13. The autocorrelation functions for the processes with logarithmic singularities in return times constructed with the special flows over the Feigenbaum (a) and circle (c) maps. The corresponding averaged squared correlation functions (b) and (d) decay as powers of time, indicating the existence of singular continuous spectrum.

V. MULTIFRACTAL PROPERTIES OF SINGULAR CONTINUOUS SPECTRA

In this section we develop a practical method for the computation of the multifractal properties of a singular continuous spectrum, and apply it to the cases considered above (see also Ref. [39]). First of all, we would like to remind the reader of the well-known thermodynamic formalism for fractal measures (see, e.g., [40]). For simplicity we consider a power spectrum of a discrete-time process; this spectrum is defined in the interval $0 \le \omega \le 1$. Dividing this interval into L subintervals with sizes $\varepsilon = L^{-1}$, and denoting their measures as p_k, we can write the coarse-grained partition function as

$$\Gamma(\varepsilon, q) = \sum_{1}^{L} p_k^q , \tag{9}$$

and its growth rate

$$\Gamma(\varepsilon, q) \sim \varepsilon^{\tau(q)} \tag{10}$$

defines the function $\tau(q)$. The generalized dimensions D_q and the $f(\alpha)$ spectrum are related to this function as

$$D_q = (q-1)^{-1}\tau(q) ,$$

$$f(\alpha) = q\alpha - \tau(q) , \quad \alpha = d\tau/dq .$$

Let us now turn to a practical calculation of the power spectrum. Given a times series x_n we can define for a frequency ω a finite-time power spectrum as

$$S(T,\omega) = \frac{1}{T}\left\langle \left| \sum_{1}^{T} x_n e^{i2\pi\omega n} \right|^2 \right\rangle .$$

This value grows with time T as

$$S(T,\omega) \sim T^{\lambda(\omega)} ,$$

where λ determines the strength of the spectral peak at the frequency ω. Respectively, λ can be viewed as the Lyapunov exponent of the spectrum at a given frequency; its existence may be questionable for some particular ω,

but according to [41] it exists for a set of full measure. The value of the Lyapunov exponent λ determines the strength of the spectral peak at the frequency ω. Thus $\lambda=1$ corresponds to a δ peak in the spectrum, while for a broadband spectrum $\lambda=0$; for a singular continuous spectrum generally $\lambda\neq 0, 1$. Averaging over the frequencies we can define the function $\sigma(q)$ as

$$\int_0^1 S^q(T,\omega)d\omega \sim T^{\sigma(q)} . \tag{11}$$

The spectrum of local Lyapunov exponents [42] is related to $\sigma(q)$ via the Legendre transform

$$g(\Lambda)=\sigma(q)-q\Lambda , \quad \Lambda=d\sigma/dq .$$

We now derive a relation between the spectrum of the local Lyapunov exponents $g(\Lambda)$ and the $f(\alpha)$ spectrum. The estimation of the finite-time power spectrum makes sense only for the discrete set of frequencies: $\omega_k=(k-1)T^{-1}$. The obtained values of the power spectrum can be considered as a coarse-grained estimate to the measure: $p_k \approx S(T,\omega_k)T^{-1}$, $\varepsilon=T^{-1}$. Substituting this expression into (9) and (10) and comparing with (11) we get [43]

$$\sigma(q)=q-1-\tau(q) . \tag{12}$$

For Legendre transforms this immediately gives [44]

$$\alpha=1-\Lambda , \quad f(\alpha)=1+g(\Lambda) . \tag{13}$$

The relations (12) and (13) provide a simple method for calculation of the generalized dimensions and $f(\alpha)$ spectrum of the singular continuous spectrum, using finite-time estimations of the power spectrum (11).

We have applied the method described to the spectra discussed in Sec. III. These power spectra, being obtained for the continuous-time dynamical system, are defined for all frequencies. The tail at large frequencies decays, however, exponentially. Therefore it is convenient to restrict the integral (11) to an interval in the frequency domain, containing major peaks. Calculations of the $f(\alpha)$ spectrum, performed in this way, are presented in Fig. 14.

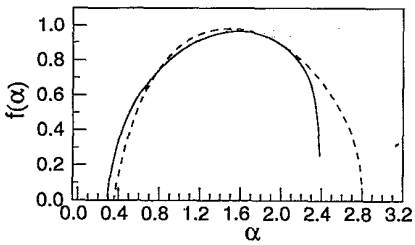

FIG. 14. The $f(\alpha)$ spectra for the singular continuous power spectra of the variable z in the system (6) for the attractors Fig. 2 (dashed line) and Fig. 9 (solid line).

VI. CONCLUSIONS

In this paper we have demonstrated that singular continuous spectra can be observed in certain autonomous dissipative dynamical systems at the point of transition to chaos. In the investigated ODE system we found two different mechanisms which are responsible for these spectra. The first mechanism, being purely geometrical, works equally well for both discrete-time and continuous-time dynamics; it is connected with the appearance of the particular symbolic code—the Thue-Morse sequence (or its generalizations). The second mechanism which owes to the dynamics of the return times affects only the continuous-time systems and is connected with singular phase modulation, when the process consists of pulses of different length. The amplitudes of the pulses are described by a corresponding Poincaré map and behave quasiperiodically (when the map is equivalent to a circle map with irrational rotation number) or almost periodically (when the map has the Feigenbaum-like attractor). The singular continuous spectrum appears when the dependence of the duration of pulses on their amplitude has a logarithmic singularity. Such a singularity is present in the considered ODE system because the closure of the attractor includes the saddle point, in which neighborhood the trajectories "stick" for a long time. As a consequence, the spectral properties of the continuous flow differ from those of the mapping. From the results of von Neumann [36] it follows that the singularity of phase modulation may be even weaker, in some cases a discontinuity in the dependence of return time on the amplitude is enough for the spectrum to be continuous. It is remarkable that the atomic lattices with singular continuous spatial spectrum discussed in Refs. [5–7] can be constructed with the help of a special flow having such a discontinuity (see Appendix B). Presently, however, we do not have an example of an autonomous dynamical system in which a discontinuity of return times is responsible for a singular continuous spectrum.

ACKNOWLEDGMENTS

We thank M. Combescure, P. Grassberger, K. Khanin, V. Oseledec, A. Politi, M. Rosenblum, D. Shepelyansky, and U. Smilansky for useful discussions. M. Z. acknowledges support from the Max-Planck-Gesellschaft.

APPENDIX A: THE THUE-MORSE SEQUENCE

In this section we discuss spectral properties of the Thue-Morse sequence [17,18,20]. The Thue-Morse sequence is an infinite sequence of two symbols, say a and b, defined by the following substitution (inflation) rule:

$$a \to ab , \quad b \to ba . \tag{A1}$$

Starting with a we get consequently a, ab, $abba$, $abbabaab$, etc. For the computation of the Fourier spectrum it is useful to mention that the sequence can be also obtained from the concatenation rule

$$A \to A\bar{A} , \tag{A2}$$

where the overbar denotes the inverse (with symbols a and b interchanged) sequence. Putting 1 instead of a and -1 instead of b, we obtain a sequence x_k with zero average: $\langle x_k \rangle = 0$. We define the partial Fourier sum of the first 2^n elements as

$$Z_n(\omega) = 2^{-n/2} \sum_{k=1}^{2^n} x_k e^{ik2\pi\omega} .$$

Dividing this sum into two halves and using the concatenation rule (which implies $x_{2^{n-1}+k} = -x_k$) we arrive at the recursion relation

$$Z_n(\omega) = Z_{n-1}(\omega) \frac{1 - e^{i2^{n-1}2\pi\omega}}{2^{1/2}} .$$

For the power spectrum $S_n(\omega) = |Z_n(\omega)|^2$ we get

$$S_{n+1}(\omega) = S_n(\omega)[1 - \cos(2\pi 2^n \omega)] .$$

(Note that we can rewrite this recurrence as

$$S_{n+1}(\omega/2) = S_n(\omega)[1 - \cos(\pi\omega)] \quad \text{(A3)}$$

which explains the observed self-similarity of the spectrum Fig. 5 in the region of small frequencies.) Thus the spectral measure is represented as an infinite product (Riesz product [20]):

$$\mu(\omega) = \lim_{n\to\infty} S_n(\omega) = \lim_{n\to\infty} \prod_{k=0}^{n-1} [1 - \cos(2\pi 2^k \omega)] . \quad \text{(A4)}$$

The Riesz product provides a simple tool for finding the multifractal properties of the spectrum, as described in Sec. V. The finite product $S_n(\omega)$ corresponds to the finite-time power spectrum at time 2^n. The Lyapunov exponents $\lambda(\omega)$ can be found from the simple dynamical system

$$S_{n+1} = S_n[1 - \cos(2\pi\phi_n)] , \quad \text{(A5)}$$

$$\phi_{n+1} = 2\phi_n \pmod 1 \quad \text{(A6)}$$

with initial condition $S_0 = 1$, $\phi_0 = \omega$. Thus the exponent $\lambda(\omega)$ appears as a logarithm of the multiplicator along the trajectory of transformation (A5), (A6) For the periodic orbits in (A6) the calculation is trivial: $\lambda(1/3) = \Lambda_{\max} = \log(3/2)/\log(2) \approx 0.584$, $\lambda(1/5) \approx 0.16$, $\lambda(1/9) \approx -0.47$, etc. Note also that all the frequencies that are attracted eventually to a periodic orbit have the same exponent [e.g., $\lambda(1/6) = \lambda(1/12) = \cdots = \lambda(1/3)$], whereas the transient part of the orbit determines the ratio of the spectral peaks growing with the same exponential rate (e.g., $S_n(1/3)/S_n(1/6) = [1 - \cos(2\pi/3)]/[1 - \cos(2\pi/6)] = 3$). Note also that $\Lambda_{\min} = \lambda(0) = -\infty$. The $f(\alpha)$ spectrum is restricted, according to (13), to the domain $1 - \Lambda_{\max} \approx 0.42 < \alpha < \infty$ (see Fig. 7 in [39]).

We now discuss the properties of the autocorrelation function for the Thue-Morse sequence. It is presented in Fig. 15. First, we would like to note that in contrast to the power spectrum, the values of the autocorrelation function are well defined for each time t. The self-similar structure of the autocorrelation function is clearly seen when the time scale is logarithmic [Fig. 15(b)]. The logarithmic periodicity of main peaks can be explained as follows: from the fact that the Thue-Morse sequence is invariant with respect to decimation (deletion of each second element), it follows immediately that

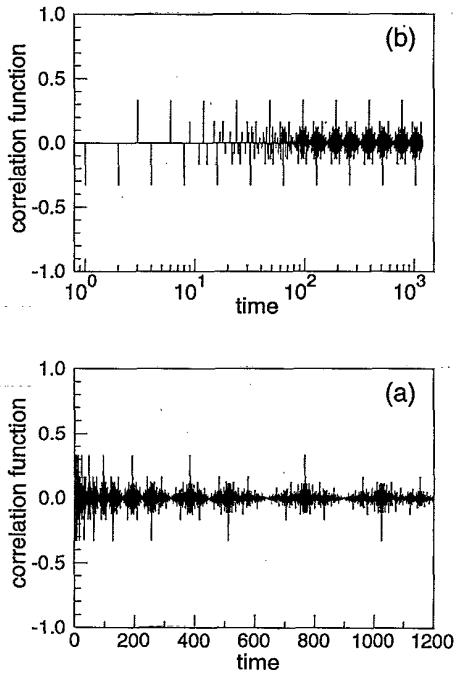

FIG. 15. The autocorrelation function of the Thue-Morse sequence. The self-similar structure is well seen when the time scale is logarithmic (b).

$$C(2t) = C(t) .$$

Using the Riesz product (A4) one can deduce a recurrence relation for the autocorrelation function. Although they are suitable for numerical calculations, analytical formulas are rather cumbersome; however, for small t the values of correlation are not difficult to obtain: $C(1) = -1/3 = -C(3)$.

Another scaling property of the autocorrelation function is illustrated in Fig. 16. Here the part near one of the main peaks at $t = 1024$ is compared with the part at $t = 0$. One can see that the correlations scale. Generally, we can show that

$$C(2^n + l) \approx C(2^n) C(l) \quad \text{(A7)}$$

if $l \ll 2^n$. Indeed, let us take the Thue-Morse sequence of length $N = M2^l$, $M \gg 1$ and write the correlation function $C(2^n + l)$ as

$$C(2^n + l) = \frac{1}{(M-1)2^n - l} \sum_{k=1}^{(M-1)2^n - l} x_k x_{k+2^n+l} .$$

Now we use the condition $l \ll 2^n$ and exclude from each block of length 2^n the last l elements [this means that we exclude from the sum $l(M-1)$ elements corresponding to overlapping between the blocks]:

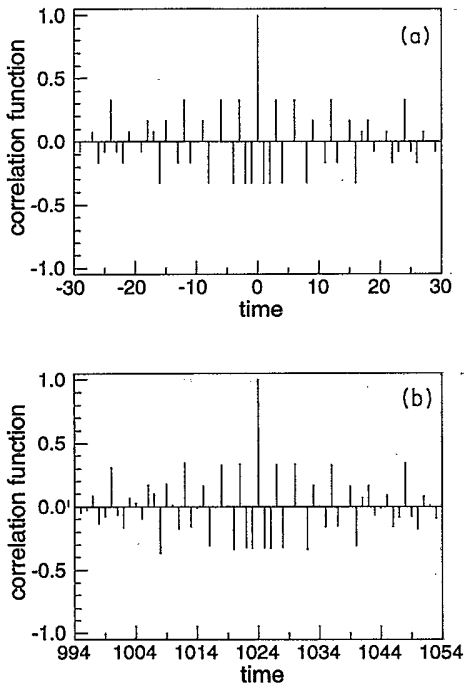

FIG. 16. Self-similar structure of the autocorrelation function Fig. 15. The part near $t=1024$ is multiplied by $-3=1/C(1024)$, and plotted under the part adjacent to $t=0$.

$$C(2^n+l)\approx \frac{1}{(M-1)}\frac{1}{(2^n-l)} \times \sum_{m=1}^{M-1}\sum_{k=(m-1)2^n+1}^{m2^2-l}(x_k x_{k+2^n})(x_{k+2^n}x_{k+2^n+l}) . \tag{A8}$$

Due to the way of the construction of the Thue-Morse sequence (A2), the values of $x_{k+2^n}x_{k+2^n+l}$ are the same for all blocks, and inside any block the value of $x_k x_{k+2^n}$ is constant, so we can rewrite (A8) as

$$C(2^n+l)\approx \left[\frac{1}{2^n-l}\sum_{k=1}^{2^n-l}x_k x_{k+l}\right] \times \left[\frac{1}{M-1}\sum_{m=1}^{M-1}x_{(m-1)2^n+1}x_{(m-1)2^n+1+2^n}\right] .$$

Here the first term in large parentheses is approximately $C(l)$ and the second term in large parentheses can be considered as a correlation function of a decimated Thue-Morse sequence, where only each 2^n-th element is taken. Because the Thue-Morse sequence is invariant under the decimation, the second term gives $C(1)=C(2^n)$. Thus we get the scaling relation (A7).

APPENDIX B: SPECIAL FLOWS AND COMPLEX SPATIAL STRUCTURES

In Refs. [5,7] the following one-dimensional chain of atoms was considered. The abscissa u_n of the nth atom is defined through $u_{n+1}-u_n=l_n$ where the bond lengths l_n can be equal either 1 or $1+\xi$ (the parameter ξ defines the strength of modulation) according to

$$l_n=\begin{cases}1+\xi & \text{if } 0\le \mathrm{frac}(nl)<\Delta ,\\ 1 & \text{if } \Delta\le \mathrm{frac}(nl)<1 ,\end{cases} \tag{B1}$$

where $\mathrm{frac}(x)$ denotes the fractional part of x. Here l is irrational and Δ is a parameter. This definition can be rewritten as

$$l_n=F(x_n) , \quad x_{n+1}=x_n+l \bmod 1 \tag{B2}$$

with a piecewise constant function $F(x)$ having values $1+\xi$ and 1 on the intervals $0\le x<\Delta$ and $\Delta\le x<1$. Comparing this construction with the definition of the special flow (8), one can see that the special flow with the circle map $f(x)=x+l \bmod 1$ and the corresponding $F(x)$ produces the bond lengths l_n as the return times. Thus, the chain of atoms constructed in [5,7] can be considered as the sequence of δ pulses produced by the special flow.

[1] P. Bergé, Y. Pomeau, and C. Vidal, *Order Within Chaos* (Wiley, New York, 1986).
[2] H. G. Schuster, *Deterministic Chaos, An Introduction* (VCH-Verlag, Wienheim, 1988).
[3] A. J. Lichtenberg and M. A. Lieberman, *Regular and Chaotic Dynamics* (Springer, New York, 1992).
[4] J. Argyris, G. Faust, and M. Haase, *An Exploration of Chaos* (North-Holland, Amsterdam, 1994).
[5] S. Aubry, C. Godrèche, and J. M. Luck, Europhys. Lett. **4**, 639 (1987).
[6] C. Godrèche, J. M. Luck, and F. Vallet, J. Phys. A **20**, 4483 (1987).
[7] S. Aubry, C. Godrèche, and J. M. Luck, J. Stat. Phys. **51**, 1033 (1988).
[8] R. Artuso *et al.*, Int. J. Mod. Phys. B **8**, 207 (1994).
[9] J. M. Luck, H. Orland, and U. Smilansky, J. Stat. Phys. **53**, 551 (1988).
[10] U. Feudel, A. S. Pikovsky, and M. A. Zaks, Phys. Rev. E **51**, 1762 (1995).
[11] A. Pikovsky and U. Feudel, J. Phys. A **27**, 5209 (1994).
[12] D. V. Lyubimov and M. A. Zaks, Physica D **9**, 52 (1983).
[13] A. Arneodo, P. Coullet, and C. Tresser, Phys. Lett. A **81**, 197 (1981).
[14] J.-M. Gambaudo, I. Procaccia, S. Thomae, and C. Tresser, Phys. Rev. Lett. **57**, 925 (1986).
[15] I. Procaccia, S. Thomae, and C. Tresser, Phys. Rev. A **35**, 1884 (1987).
[16] D. V. Lyubimov, A. S. Pikovsky, and M. A. Zaks, in *Sov. Sci. Rev., Mathematical Physics Review,* edited by S. P. Novikov (Harwood Academic, Chur, Switzerland, 1989), Vol. 8, pp. 221–292.
[17] A. Thue, Norske Vidensk. Selsk. Skr. I. Mat. Nat. Kl. Christiania **7**, 1 (1906).
[18] M. Morse, Trans. Am. Math. Soc. **22**, 84 (1921).

[19] I. P. Cornfeld, S. V. Fomin, and Ya. G. Sinai, *Ergodic Theory* (Springer, New York, 1982).
[20] M. Queffélec, *Substitution Dynamical Systems—Spectral Analysis,* Lecture Notes in Mathematics Vol. 1294 (Springer, Berlin, 1987).
[21] H. Broer and F. Takens, Arch. Rational Mech. Anal. **124,** 13 (1993).
[22] R. Ketzmerick, G. Petschel, and T. Geisel, Phys. Rev. Lett. **69,** 695 (1992).
[23] M. Holschneider, Commun. Math. Phys. **160,** 457 (1994).
[24] K. A. Makarov, J. Math. Anal. Appl. **187,** 259 (1994).
[25] G. Z. Gershuni and E. M. Zhukhovitsky, *Convective Stability of Incompressible Fluid* (Keter, Jerusalem, 1976).
[26] V. S. Afraimovich, V. V. Bykov, and L. P. Shilnikov, Dokl. Akad. Nauk. SSSR **234,** 336 (1977) [Sov. Phys. Dokl. **22,** 253 (1977)].
[27] C. Sparrow, *The Lorenz Equations: Bifurcations, Chaos, and Strange Attractors* (Springer, Berlin, 1982).
[28] M. J. Feigenbaum, Commun. Math. Phys. **77,** 65 (1980).
[29] M. A. Zaks, Physica D **63,** 300 (1993).
[30] Z. Cheng, R. Savit, and R. Merlin, Phys. Rev. B **37,** 4375 (1988).
[31] F. Axel and H. Terauchi, Phys. Rev. Lett. **66,** 2223 (1991).
[32] M. Combescure, J. Stat. Phys. **62,** 779 (1991).
[33] Although in real systems the Poincaré map is invertable, at the point of accumulation of period doublings it can be well approximated with a one-dimensional parabola-type mapping.
[34] A. N. Kolmogorov, Dokl. Akad. Nauk. SSSR **93,** 763 (1953).
[35] A. S. Pikovsky, Radiophys. Quantum Electron. **29,** 1076 (1986).
[36] J. von Neumann, Ann. Math. **33,** 587 (1932).
[37] A. V. Kochergin, Math. Notes **19,** 277 (1976).
[38] Ya. G. Sinai and K. M. Khanin, Funct. Anal. Appl. **26,** 1 (1992).
[39] C. Godrèche and J. M. Luck, J. Phys. A **23,** 3769 (1990).
[40] T. Bohr and T. Tél, in *Directions in Chaos,* edited by H. B.-Lin (World Scientific, Singapore, 1988), pp. 195–237.
[41] V. I. Oseledec, Trans. Moscow Math. Soc. **19,** 197 (1968).
[42] A. Crisanti, G. Paladin, and A. Vulpiani, *Products of Random Matrices in Statistical Physics* (Springer, Berlin, 1993).
[43] A particular case $q=\frac{1}{2}$ has been discussed in Ref. [5].
[44] A. Politi (private communication).
[45] W. H. Press, B. P. Flannery, S. A. Teukolsky, and W. T. Vetterling, *Numerical Recipes* (Cambridge University Press, Cambridge, 1989).